JACS
JOURNAL OF THE AMERICAN CHEMICAL SOCIETY

Article

pubs.acs.org/JACS

Optimized End-Stacking Provides Specificity of *N*-Methyl Mesoporphyrin IX for Human Telomeric G-Quadruplex DNA

John M. Nicoludis,[†,∥] Stephen T. Miller,[†] Philip D. Jeffrey,[‡] Steven P. Barrett,[†] Paul R. Rablen,[†] Thomas J. Lawton,[§] and Liliya A. Yatsunyk*[,†]

[†]Department of Chemistry and Biochemistry, Swarthmore College, 500 College Avenue, Swarthmore, Pennsylvania 19081, United States

[‡]Department of Molecular Biology, Princeton University, Lewis Thomas Laboratory, Washington Road, Princeton, New Jersey 08544-1014, United States

[§]Departments of Molecular Biosciences and of Chemistry, Northwestern University, Evanston, Illinois 60208, United States

Supporting Information

ABSTRACT: *N*-Methyl mesoporphyrin IX (NMM) is exceptionally selective for G-quadruplexes (GQ) relative to duplex DNA and, as such, has found a wide range of applications in biology and chemistry. In addition, NMM is selective for parallel versus antiparallel GQ folds, as was recently demonstrated in our laboratory. Here, we present the X-ray crystal structure of a complex between NMM and human telomeric DNA dAGGG(TTAGGG)$_3$, Tel22, determined in two space groups, $P2_12_12$ and P6, at 1.65 and 2.15 Å resolution, respectively. The former is the highest resolution structure of the human telomeric GQ DNA reported to date. The biological unit contains a Tel22 dimer of 5′-5′ stacked parallel-stranded quadruplexes capped on both ends with NMM, supporting the spectroscopically determined 1:1 stoichiometry. NMM is capable of adjusting its macrocycle geometry to closely match that of the terminal G-tetrad required for efficient $\pi-\pi$ stacking. The out-of-plane *N*-methyl group of NMM fits perfectly into the center of the parallel GQ core where it aligns with potassium ions. In contrast, the interaction of the *N*-methyl group with duplex DNA or antiparallel GQ would lead to steric clashes that prevent NMM from binding to these structures, thus explaining its unique selectivity. On the basis of the biochemical data, binding of NMM to Tel22 does not rely on relatively nonspecific electrostatic interactions, which characterize most canonical GQ ligands, but rather it is hydrophobic in nature. The structural features observed in the NMM−Tel22 complex described here will serve as guidelines for developing new quadruplex ligands that have excellent affinity and precisely defined selectivity.

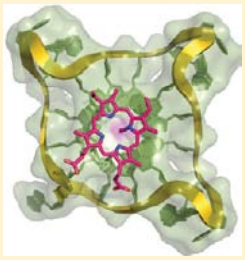

INTRODUCTION

G-Quadruplex (GQ) DNA structures potentially exist at the telomeres of eukaryotic chromosomes, as their repetitive G-rich sequences (e.g., TTAGGG in mammals) are known to adopt such noncanonical DNA structures in vitro. GQs are made by $\pi-\pi$ stacking of the G-tetrads (Figure 1a), each formed by four guanines held together by Hoogsteen hydrogen bonds and stabilized by a central monovalent metal cation. Various forms of the human telomeric GQs have been structurally characterized by NMR and X-ray crystallography.[1] In the crystalline state, human telomeric DNA preferentially folds into an all-parallel conformation with three TTA propeller loops (Figure 1b).[2] Under dilute solution conditions in Na^+ buffer, telomeric DNA folds into an antiparallel conformation,[3] and in K^+ buffer it adopts three mixed-polarity conformations depending on the exact sequence.[1] In solution, the all-parallel propeller loop GQ structure can be induced by polyethylene glycol (PEG), ethanol, high DNA concentration ([nucleoside] > 100 mM),[4,5] or *N*-methyl mesoporphyrin IX (NMM).[6]

GQ structures can be stabilized by small molecule ligands[7,8] including porphyrins.[9] Ligands that can selectively stabilize GQs, but not double-stranded DNA (dsDNA), may have potential applications as pharmaceuticals for cancer therapy. GQ ligands may inhibit tumor growth by disrupting telomere structures, thus triggering cellular responses that lead to senescence or apoptosis.[10] GQ binders are also finding applications in nanotechnology,[11] in analytical chemistry for sensing,[12] in biology for in vivo GQ detection,[13,14] and in other fields of science.

The Protein Data Bank contains 130 high-resolution structures of GQs. However, only 13 reveal the molecular architecture of human telomeric quadruplexes (both DNA and RNA) in complexes with ligands, of which 11 were determined by X-ray crystallography. These ligands include a set of tetra-substituted naphthalene diimide compounds,[15,16] nickel and copper salphen complexes,[17] an acridine compound,[18] berberine,[19] BRACO-19,[20] and a well-studied porphyrin, TMPyP4.[21] With the exception of TMPyP4, the ligands stack onto a G-tetrad. Available crystal structures have revealed some elements required for efficient quadruplex stabilization by a small molecule; however, the limited number of crystal structures and, in some cases, their relatively low resolution have prevented generalization of these features.[20,22−24] In addition,

Received: September 6, 2012
Published: November 26, 2012

dx.doi.org/10.1021/ja3088746 | J. Am. Chem. Soc. 2012, 134, 20446−20456

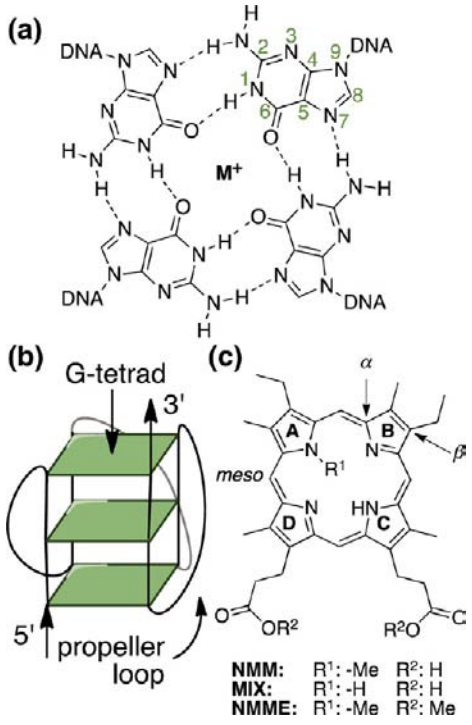

Figure 1. Structure of a G-tetrad and NMM. (a) Schematic representation of a G-tetrad including numbering of the atoms of one guanine. (b) A parallel G-quadruplex. (c) Structure of *N*-methyl mesoporphyrin IX, NMM. Only one of the four regioisomers of NMM is shown; regioisomers differ by which pyrrole nitrogen (A–D) bears the *N*-Me group. Replacing the *N*-Me group in NMM with a hydrogen atom yields the structure of mesoporphyrin IX, MIX.

most of the crystallized ligands have only moderate selectivity for GQs over dsDNA. Structural information on highly GQ-selective ligands, their mode of binding to quadruplex DNA, and knowledge of molecular features required for selectivity will be invaluable for future ligand design.

Recently, our group conducted an in-depth biophysical investigation of interactions between NMM, shown in Figure 1c, and human telomeric DNA, dAGGG(TTAGGG)$_3$, Tel22.[6] First identified as a GQ binder through a SELEX approach to find porphyrin aptamers,[25] NMM displayed exceptional selectivity for GQ versus dsDNA in competition dialysis and fluorescence studies[22,26] and, based on this property, is currently widely used in chemistry and biology.[27−29] Even more interestingly, our laboratory was able to demonstrate that NMM has the unique ability to recognize parallel-stranded but not antiparallel GQ structures.[6] The molecular basis for such selectivity requires further investigation. It is important to note that the commercially available NMM is a racemic mixture of eight isomers: four regioisomers, which differ in the position of the *N*-Me group, each of which has a pair of enantiomers that differ in the side of the macrocycle from which the *N*-Me group protrudes. The enantiomers do not easily interconvert at ordinary temperatures; the free energy barrier to racemization is calculated to be 54.3 kcal mol^{-1} (full details of the calculation appear in the Supporting Information). All of the reported biological and biochemical studies involving NMM were performed using this isomer mixture. To better inform these studies, our laboratory set out to characterize the interaction of Tel22 with the isomer mixture of NMM, rather than focus on separate isomers.

In this work, we present the crystal structure of the NMM–Tel22 complex solved in two space groups, $P2_12_12$ and *P6*, at resolutions of 1.65 and 2.15 Å, respectively (Figure 2). The $P2_12_12$ structure is the highest resolution structure of the human telomeric GQ DNA reported to date. Tel22 forms a dimer of 5′-5′ stacked intramolecular parallel quadruplexes with NMM bound to the 3′-terminal G-tetrads. The structure displays optimized surface complementarity between NMM and the 3′ G-tetrad, which results from GQ-induced distortion of the porphyrin macrocycle. The *N*-methyl (*N*-Me) group of NMM points directly into the center of the quadruplex core and is aligned with the column of potassium ions. The binding of NMM to duplex or antiparallel GQ is inhibited due to steric clashes involving this *N*-Me group. Results of our work, thus, provide framework for understanding how NMM interacts with Tel22 and will inform the design of highly selective GQ ligands.

MATERIALS AND METHODS

Porphyrins and Oligonucleotides. The oligonucleotide dAGGG(TTAGGG)$_3$ (Tel22) was purchased from Midland Certified Reagent Co. and used without further purification. The concentration of Tel22 was determined spectroscopically using an extinction coefficient of 228.5 mM^{-1} cm^{-1} at 260 nm.[30] NMM and its dimethyl ester (NMME) were purchased from Frontier Scientific. The concentrations of porphyrins were determined using extinction coefficients of 1.45 × 10^5 M^{-1} cm^{-1} at 379 nm in H_2O[22] for NMM and 1.156 × 10^5 M^{-1} cm^{-1} at 410.5 nm in DMSO (determined in this work, see Supporting Information Figure S1) for NMME.

Crystallography. Tel22 and NMM were mixed and diluted to concentrations of 1.2 and 2.4 mM, respectively, in 10 mM lithium cacodylate buffer, pH 7.2, 50 mM LiCl, and 50 mM KCl, annealed at 90 °C for 10 min, slowly cooled to 30 °C, and incubated at this

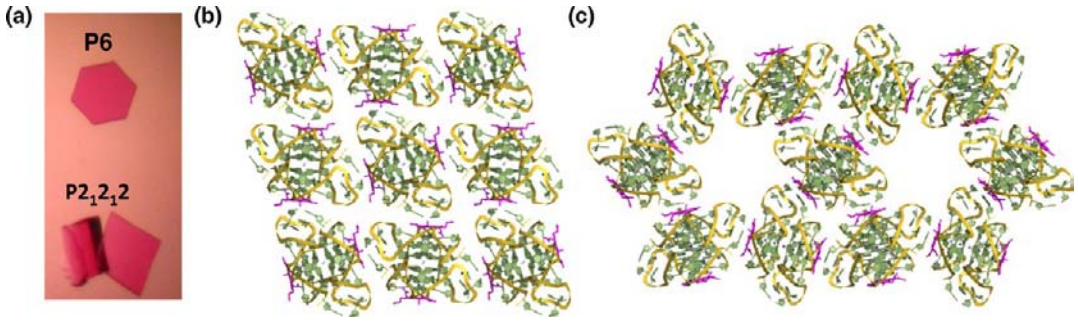

Figure 2. NMM–Tel22 crystals and crystal packing. (a) Representative image of hexagonal and rhombic crystals of the NMM–Tel22 complex. Extended arrangements of Tel22–NMM complexes within the (b) $P2_12_12$ or (c) *P6* crystal lattices. The DNA bases are shown in green, the backbone in yellow, and NMM in magenta.

dx.doi.org/10.1021/ja3088746 | J. Am. Chem. Soc. 2012, 134, 20446–20456

temperature for 30 h. Crystals were grown using hanging drop vapor diffusion methods at 4 °C. Crystals in the $P2_12_12$ space group (crystal form **1**) were obtained using the well solution of 0.05 M lithium cacodylate buffer, pH 7.2, 0.40 M ammonium sulfate, 0.05 M KCl, 0.01 M $CaCl_2$, and 15% PEG400; crystals in the *P*6 space group (crystal form **2**) were obtained using the well solution of 0.05 M lithium cacodylate buffer, pH 7.2, 0.625 M ammonium acetate, 0.20 M KCl, and 15% PEG400. One microliter of sample was mixed with 0.5 or 0.75 μL of well solution for crystal forms **1** and **2**, respectively. Crystals grew in a week as hexagonal or rhombic prisms (Figure 2a); they were harvested and cryoprotected in a solution of the mother liquor with an additional 15% PEG400, bringing total PEG400 concentration to 30%.

Data were collected at NSLS Beamline X29 at Brookhaven National Laboratories using an ADSC 315r detector (for crystal form **1**) and at LS-CAT sector 21 line G at Argonne National Laboratories using a MAR 300 CCD (for crystal form **2**). Diffraction data were processed with MOSFLM.[31] The structures were solved via molecular replacement using PHENIX[32] with the DNA G-quadruplex from PDB entry 3T5E as the search model. Models were built using iterative cycles of building in Coot[33] and refinement in PHENIX followed by final refinement in REFMAC5.[34] The ligand was placed using the automated LigandFit PHENIX module and subsequently refined using PHENIX and REFMAC5. Refinement statistics and final geometries are given in Table 1. For details on Tel22 hydration sphere, see Supporting Information Figure S2.

Table 1. Crystallographic Statistics for NMM−Tel22 Complex

	crystal form **1**	crystal form **2**
space group	$P2_12_12$	*P*6
unit cell dimensions		
a, *b*, *c* (Å)	50.755, 41.980, 42.384	64.200, 64.200, 42.360
α, β, γ (deg)	90, 90, 90	90, 90, 120
resolution (Å)	42.38−1.65	42.36−2.15
(highest resolution shell)	(1.74−1.65)	(2.27−2.15)
R_{merge} (%) overall	9.9 (46.2)	6.6 (63.8)
I/σ	11.1 (2.8)	12.8 (2.5)
completeness (%)	99.83 (98.2)	98.8 (84.4)
redundancy	8.0 (6.3)	7.9 (6.7)
refinement		
resolution (Å)	42.38−1.65	42.36−2.15
reflections	10 820	5056
R_{work}/R_{free} (%)	22.21/26.18	23.79/26.21
no. of atoms	570	518
ions	3	3
water	53	7
overall *B*-factor (Å^2)	34.223	53.195
rms deviations		
bond lengths (Å)	0.020	0.013
bond angles (deg)	3.668	3.643
PDB ID	4FXM	4G0F

Molecular graphics and structure alignments were produced using PyMOL.[35] For alignment, PyMOL's built-in Pair_Fit function was used, which aligned all 465 atoms of native Tel22 (PDB ID 1KF1) to the structures of the Tel22−ligand complexes. In the case of BMSG-SH-3 (PDB ID 3SC8), the 21 nucleotides (447 atoms) were aligned with nucleotides 2−22 of 1KF1. Structure factors and coordinates for NMM−Tel22 complex in $P2_12_12$ and *P*6 space groups have been deposited in the Protein Data Bank with accession codes of 4FXM and 4G0F, respectively.

Calculations. Energy-minimization calculations were used to obtain the solution- and gas-phase structures of NMM and mesoporphyrin IX (MIX). The X-ray structure coordinates of NMM from **1** were used as a starting point, with hydrogen atoms added at idealized positions. The initial MIX structure was generated by replacing the methyl group of NMM with a hydrogen atom. The geometry was optimized without constraint in the gas phase and in the presence of a simulated water solvent at B3LYP/6-31G(d).[36] All stationary points were verified via the calculation of vibrational frequencies. The calculation in the presence of a simulated solvent was performed using the Polarizable Continuum Model with integral equation formalism.[37] This model treats the solvent as a continuum characterized by a dielectric constant and having a cavity to accommodate the solute. The transition structure for NMM racemization was located using a manually generated initial guess and was verified using a frequency calculation (one imaginary frequency, with the correct motion) and intrinsic reaction coordinate (IRC) following (IRC pathways led to the two enantiomers of NMM).[38] All calculations were carried out using the Gaussian 09 package.[39]

Normal-Coordinate Structural Decomposition. NMM distortion was calculated using the normal-coordinate structural decomposition (NSD) engine.[40] In short, this software quantifies the in-plane and out-of-plane distortions of a porphyrin macrocycle from its structural coordinates (24 atoms). The out-of-plane porphyrin distortion can be represented as a linear combination of the six lowest-frequency normal deformations: saddled (B_{2u}), ruffled (B_{1u}), domed (A_{2u}), waved in *x* ($E_{g(x)}$) and in *y* directions ($E_{g(y)}$), and propeller (A_{1u}). The total out-of-plane deviation (D_{oop}) is calculated as the root-sum-square (rss) of the component deviations (d_{oop}) from an idealized planar D_{4h}-symmetric porphyrin.

Principal Component Analysis. Out-of-plane displacements for individual atoms of the NMM macrocycle and the G-tetrads were calculated using principal component analysis (PCA) in MATLAB (Mathworks). In this method, the three-dimensional coordinates of the NMM macrocycle (24 atoms) and the G-tetrads (11 atoms of each guanine group) were transformed into standard axis, where the first two components represent the in-plane vectors (the least-squares plane) and the third represents the normal vector, which signifies the out-of-plane deviations of individual atoms. Like in NSD, the D_{oop} was calculated as the rss of the deviations of individual atoms from the mean NMM or G-tetrad plane.

FRET Melting Assays. Fluorescence resonance energy transfer (FRET) melting assays were performed according to the established literature procedure[41] using doubly labeled oligonucleotide F21D, 5′-6-FAM-$G_3(TTAG_3)_3$-Dabcyl-3′, purchased from IDT. FRET competition experiments were conducted to establish the ability of NMME to differentiate between GQ and dsDNA and utilized a self-complementary 26-mer oligonucleotide 5′-CAATCGGATC-GAATTCGATCCGATTG-3′ (ds26, Midland) as a duplex competitor. FRET experiments were run in 5K buffer (10 mM lithium cacodylate, pH 7.2, 5 mM KCl, and 95 mM LiCl) using 0.2 μM of F21D.

UV−Vis and CD Studies. UV−vis spectra were collected on a Cary 300 (Varian) spectrophotometer equipped with a Peltier-thermostatted cuvette holder. UV−vis titration studies were performed by the stepwise addition of Tel22 into a solution of NMM at pH 5.8 and 8.6 as described previously.[6] CD experiments were performed on an AVIV 410 spectrometer equipped with a Peltier heating unit (temperature accuracy ±0.3 °C). CD annealing studies were performed using NMM−Tel22 and NMME−Tel22 in 5K buffer as described previously.[6] Additional experimental details can be found in the Supporting Information.

RESULTS AND DISCUSSION

Intermolecular Interactions in the Two NMM−Tel22 Structures. The structure of the NMM−Tel22 complex was solved in the $P2_12_12$ (crystal form **1**) and *P*6 (form **2**) space groups. The former is characterized by close packing interactions, whereas the latter has large solvent channels, which may lead to higher disorder and significantly lower resolution (2.15 vs 1.65 Å). It is interesting to note that the molecular symmetry is reflected in the macromolecular crystal

dx.doi.org/10.1021/ja3088746 | J. Am. Chem. Soc. 2012, 134, 20446−20456

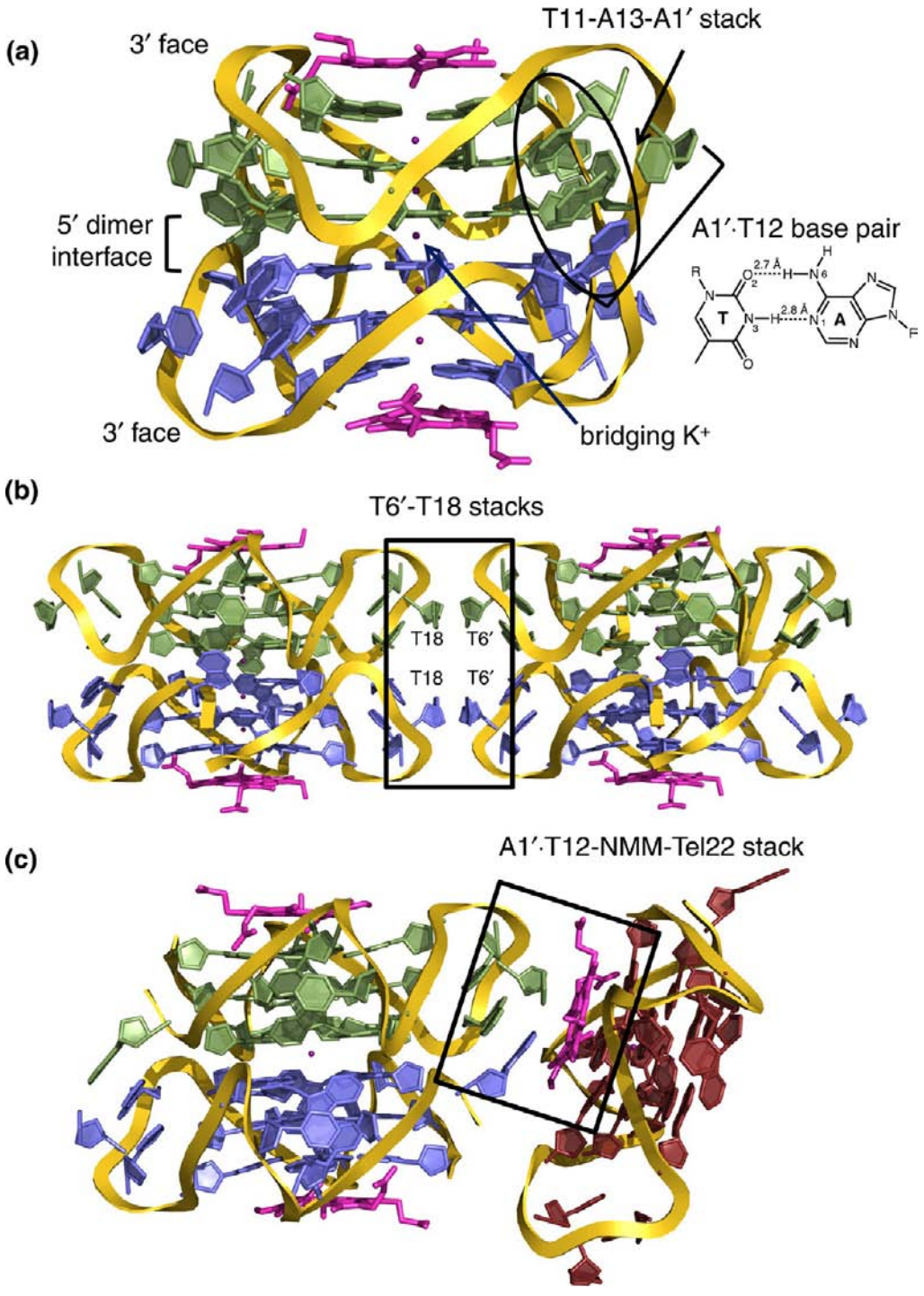

Figure 3. Intermolecular interactions in Tel22−NMM crystals. (a) Dimer formation is guided by the head-to-head stacking of 5′ G-tetrads from two intramolecular parallel GQs (green and blue), a bridging K^+ ion, an A1′·T12 base pair, and $\pi-\pi$ stacking of A1′·A13·T11 involving loops from each monomer. Interactions between dimers are mediated by (b) $\pi-\pi$ stacking of two sets of T bases and (c) stacking of NMM between the A1′·T12 base pair of one dimer (green and blue) and the 3′ G-tetrad of another (red). Reverse Watson−Crick type A−T base pair has its T rotated 180° around N3−C6 axis, as compared to conventional Watson−Crick base pair, resulting in a trans configuration of glycosyl bonds.

shape (Figure 2). Discussions in this Article focus on crystal form **1** unless otherwise noted.

In both crystal forms, Tel22 adopts a parallel propeller loop three G-tetrad quadruplex also observed in the structures of human telomeric DNA alone or with a variety of ligands.[2,15,16] This topology is most likely a result of the high DNA and K^+ concentrations required for crystal growth as well as NMM's influence on Tel22 structure. Specifically, NMM was shown to cause a structural transition of Tel22 to a parallel fold under dilute DNA and K^+ conditions.[6] Therefore, the parallel GQ core topology was expected for NMM−Tel22 crystals.

Two symmetry related Tel22 quadruplexes are arranged into a dimer, shown in Figure 3a, which is stabilized by the 5′−5′ $\pi-\pi$ stacking of G-tetrads and the bridging K^+ ion, bringing the total K^+ count to five ions per dimer. A similar dimer is also observed in the structure of Tel22 alone,[2] and complexed with

dx.doi.org/10.1021/ja3088746 | J. Am. Chem. Soc. 2012, 134, 20446−20456

naphthalene diimide ligands BMSG-SH-3 and -4.[16] The dimer is further stabilized by an A1′·T12 reverse Watson−Crick base pair (the prime (′) notation signifies that the two bases belong to separate oligonucleotide strands) with hydrogen-bonding distances of 2.7 Å for the N6 A1′···O2 T12 and 2.8 Å for the N1 A1′···N3 T12 interaction. In addition, A1′ is part of an A1′−A13−T11 $\pi-\pi$ stacked system that further stabilizes the dimer. Although the multiplicity of interactions between the monomers in the Tel22 dimer strongly hints at its stability, previous PAGE experiments have demonstrated that the NMM−Tel22 complex is monomeric in solution.[6] The observed discrepancy could originate from the drastically different experimental conditions. For crystallization, the concentration of Tel22 was 0.69−0.80 mM, and that of K^+ ions was 50 mM. In contrast, in solution studies, only 40 μM Tel22 in 5 mM KCl was loaded on a PAGE gel. To resolve this discrepancy, UV−vis and CD melting studies were performed on Tel22 samples (without NMM, see the Supporting Information for details) in the concentration range from 0.020 to 0.62 mM in the presence of 5 and 50 mM KCl. The results indicate that Tel22 is monomolecular under these conditions (Figure S3). Thus, the Tel22 dimer observed in the crystalline state is most likely due to crystal packing forces as its formation leads to a significantly reduced exposed quadruplex surface. Two neighboring dimers interact with each other via two pairs of stacked T6′−T18 bases (Figure 3b) whose planes are separated by 3.3 ± 0.1 Å. These bases are derived from the propeller TTA loops.

The Tel22 dimer is capped on both ends by NMM as shown in Figure 3a leading to a 1:1 binding stoichiometry in agreement with our earlier spectroscopic data.[6] NMM stacks onto 3′ G-tetrad, and its *N*-Me group points into the quadruplex core where it aligns with the column of K^+ ions. The other face of NMM interacts with an A1′·T12 base pair of a nearby dimer, as shown in Figure 3c. There are two choices in the stacking orientation of the A1′·T12 base pair with respect to NMM that are related by a 180° rotation around an axis perpendicular to the porphyrin plane. The choice of orientation determines the space group and leads to a specific three-dimensional arrangement of molecules in the crystal (Figure 2b and c). The stacking between the A1′·T12 base pair and NMM likely results from the crystal packing and has no (or minimal) impact on biologically significant interaction of NMM with 3′ G-tetrad as evidenced by the similar geometry of NMM in crystal forms **1** and **2** (see below).

Comparison of Native and Ligand-Bound Tel22 G-Quadruplex DNA Structures. First, the structures of the Tel22 GQs from crystal forms **1** and **2** were compared to each other. The root-mean-square deviation (rmsd) of the 465 atoms is small, 0.332 Å, suggesting a nearly identical fold. A variety of other ligands have been crystallized with the same DNA sequence: berberine,[19] naphthalene diimide ligands BMSG-SH-3 and -4,[16] and 2,7-bis[3-(dimethylamino)propyl]-4,9-bis[(3-hydroxypropyl)amino]benzo[*lmn*]-[3,8]-phenanthroline-1,3,6,8(2*H*,7*H*)-tetrone (called NII here).[15] All ligands bind to the 3′ G-tetrad of Tel22 GQ; in addition, berberine and NII intercalate into the 5′-5′ stacked Tel22 dimer and another pair of NII intercalates between loop nucleotides. These six unique Tel22 structures were aligned using PyMOL (Figure 4 and Figure S4), and the rmsd values, referenced to native Tel22 structure (PDB 1KF1), are listed in Table 2. The low values of the rmsd indicate that Tel22 in all complexes adopts a similar quadruplex fold independent of

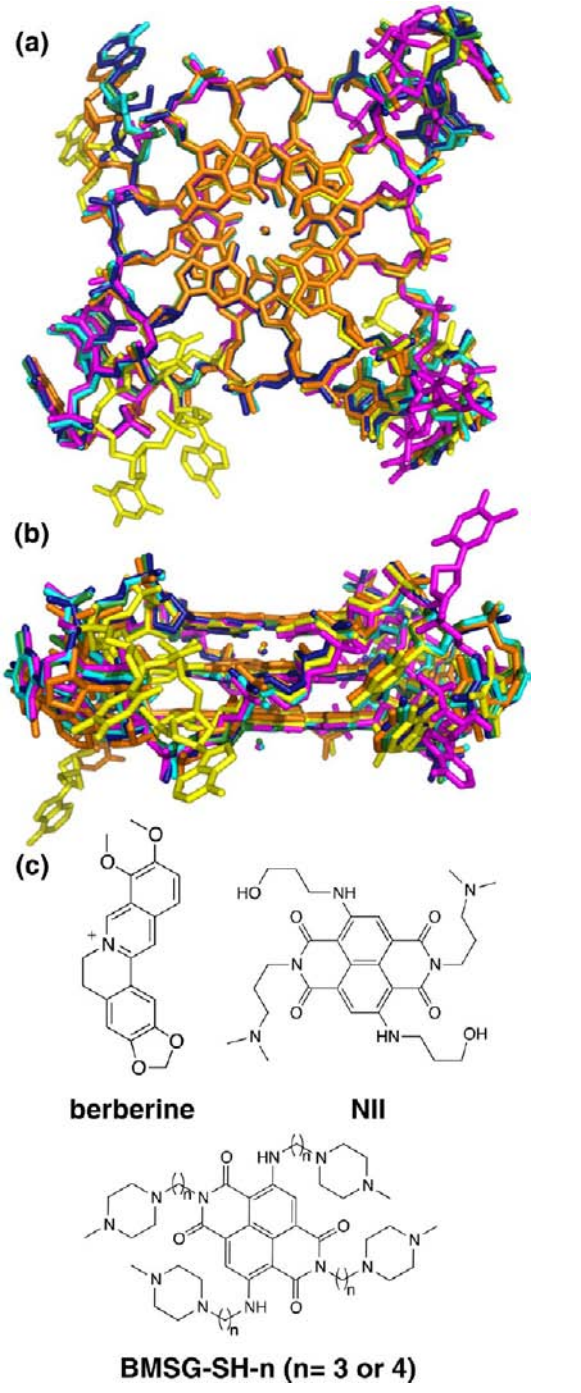

Figure 4. Alignment of native and ligand-bound Tel22 structures. (a) Top and (b) side views. Tel22 alone (PDB: 1KF1, dark blue) and with NMM (form **1**; 4FXM, green), berberine (3R6R, orange), BMSG-SH-3 (3SC8, magenta), BMSG-SH-4 (3T5E, cyan), and NII (3CDM, yellow). (c) Structures of GQ ligands.

ligand binding. The larger rmsd values seen for Tel22 in complex with the NII (2.989 Å) and BMSG-SH-3 (2.242 Å) arise mainly from variation in the TTA propeller loops. When structures of quadruplex cores are compared (using coordinates of 12 guanines), the rmsd values decrease to 0.550−0.896 Å (Table 2). The positions of the K^+ ions within the quadruplex core, the distances between the carbonyl oxygens within G-tetrads (O6−O6 distance), and the Hoogsteen hydrogen-bonding distances (N1−O6 and N2−N7) for the ligand

dx.doi.org/10.1021/ja3088746 | J. Am. Chem. Soc. 2012, 134, 20446−20456

Table 2. Root Mean Square Deviations of Ligand-Bound Tel22 As Compared to Native Tel22 (1KF1)[2]

ligand	PDB ID	rmsd, Å	core rmsd,[a] Å
NMM **1**	4FXM	0.532	0.570
NMM **2**	4G0F	0.591	0.577
NII	3CDM	2.989	0.888
berberine	3R6R	0.902	0.550
BMSG-SH-3	3SC8	2.242	0.896
BMSG-SH-4	3T5E	0.542	0.555

[a]Core rmsd is the rmsd for the 12 guanine nucleotides only.

binding 3′ G-tetrad are nearly the same for all structures (Figure S4). These results indicate that the quadruplex core geometry is well maintained in all complexes.

It was interesting to compare the mode of porphyrin binding to human telomeric quadruplex in NMM−Tel22 and TMPyP4−$(dTAG_3TTAG_3)_2$ complexes,[21] Figure S5. Unlike NMM, TMPyP4 does not interact directly with a G-tetrad; rather one molecule of TMPyP4, aligned with GQ axis, is sandwiched between A−T base pairs of two dimers, and another molecule, perpendicular to GQ axis, binds to the loops via stacking with four T bases. We believe that the ruffled geometry of TMPyP4 together with the pyridine substituents that are perpendicular to the macrocycle prevents TMPyP4 from stacking directly onto G-tetrad.

Specific Interactions between NMM and Tel22. In the crystal form **1**, the core of NMM and its *N*-Me group are well-defined, while peripheral groups, especially the propionates, are largely disordered as judged by the observed electron density and the value of the temperature (*B*) factors, Figure 5. In the

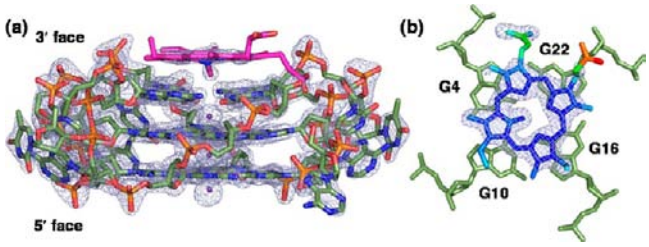

Figure 5. Details of NMM binding to Tel22. (a) Electron density map (at 2σ) and the model for the structure of crystal form **1**. The *N*-Me group of NMM is well-defined in the electron density map, indicating its unique position. (b) NMM's temperature factors, *B*, from low (blue) to high (red) shown on its electron density map (at 1σ) indicate that NMM's core has minimal amount of movement, while its peripheral substituents, especially one propionate group, are more disordered. NMM is stacked off-center, in the direction of G22, above the 3′ G-tetrad.

crystal form **2**, the core *N*-Me group is not visible in the electron density map, but the NMM macrocycle is still well-defined. Its domed distortion (see below) strongly suggests that the *N*-Me group points toward the 3′ G-tetrad. Our crystallographic data indicate that there is one possible way for NMM to bind to the Tel22 quadruplex with respect to the *N*-Me group (Figure 5), but it is not immediately clear why this orientation is preferred. It is possible that a single NMM isomer crystallizes with Tel22 or that multiple isomers bind Tel22 with identical orientations of the *N*-Me group but different placements of peripheral substituents. In an effort to identify unbiased density for the peripheral substituents of NMM, an iterative build omit map was calculated using PHENIX.[42] While the position of the *N*-Me was still clear in this map, no interpretable density for peripheral substituents was observed. Additional maps were generated in ARP/wARP[43] using the atom update and refinement module and starting models both with and without NMM; again, no clear density for side groups was observed. Thus, at this point, it is impossible to distinguish thermal motion of a single NMM isomer bound to Tel22 from multiple occupancies of more than one NMM isomer.

Using the Ligand Expo program,[44] a previously defined NMM isomer with component identifier MMP was chosen as the most appropriate NMM model, based on some evidence for the location of the propionate groups in electron density map (Figure S6). This isomer is the (*S*)-enantiomer of the regioisomer with the *N*-Me group attached to ring A (Figure 1c). It was placed automatically using the LigandFit PHENIX module in an effort to remove bias in ligand placement. The NMM model used originates from the structure of a ferrochelatase, terminal enzyme in heme biosynthesis that is responsible for iron insertion into hemes.[45]

Using our NMM−Tel22 model, we examined the specific interactions between Tel22 and NMM's macrocycle, *N*-Me group, and side chains. The macrocycle of NMM is located approximately 3.6 Å from the 3′ G-tetrad, a distance consistent with efficient $\pi-\pi$ stacking. Another porphyrin, TMPyP4, was modeled 4.2 Å above G-tetrad in its NMR structure with the *c-myc* promoter.[46] This significantly longer stacking distance could be explained by the nearly perpendicular orientations of pyridyl groups in TMPyP4 relative to the porphyrin core and steric clashes that would result from bringing this porphyrin closer to the G-tetrad. Nearly planar ligands such as berberine, two different metal−salphen complexes, and a naphthalene diimide compound are located approximately 3.4−3.6 Å away from the terminal G-tetrad.[16,17,19] Thus, the exceptional selectivity of NMM for GQ DNA does not result from its stronger stacking interaction with the 3′ G-tetrad of Tel22 as compared to other ligands.

The *N*-Me group of NMM is bent 44.8° away from the mean porphyrin plane pointing toward the 3′ G-tetrad. It is aligned with the column of K^+ ions, leading to the observed off-center position of the NMM macrocycle toward G22 (Figure 5b). Interestingly, the napahthalene diimide ligands, BMSG-SH-3[16] and BRACO-19,[20] are also stacked asymmetrically onto the human telomeric DNA. In the case of BRACO-19 complex, the off-center position is due to the optimized interactions between the cationic ring nitrogen atom of the ligand and the potassium ion channel; in the case of BMSG-SH-3, it is due to the interaction between the side-chain methyl-piperazine groups of the ligand and Tel22 grooves.

As far as peripheral substituents are concerned, clear electron density is visible for one propionate carboxylate group at 1σ. This group may participate in a hydrogen-bonding network with two backbone phosphates (in one case through a water molecule) as shown in Figure S6a, and, thus, may be protonated under crystallization conditions. The other propionate, which is only visible at 0.5σ, may interact with a 3′ sugar oxygen through a water molecule, Figure S6b. Thus, our current model supports, at least to some degree, the stereospecificity of NMM−Tel22 interactions, and Tel22's preference for one NMM isomer. It is important to note that there is no density connecting modeled carboxylate groups to the porphyrin core and the observed electron density could be equally fitted with water molecules. To resolve ambiguity concerning the stereospecificity of Tel22−NMM interactions,

dx.doi.org/10.1021/ja3088746 | J. Am. Chem. Soc. 2012, 134, 20446−20456

we are in the process of separating the isomers of NMM. Structural information on separated NMM isomers may shed light on the positions of the peripheral groups and their interactions with the GQ. If Tel22 displays a preference for one isomer over another, it might become important to use separate isomers for current applications of NMM.[27−29]

Structural Basis for Selectivity of NMM for Parallel Quadruplex DNA. Structural features of the NMM−Tel22 complex provide possible explanations for the unique selectivity of NMM for the parallel versus antiparallel topology observed in our earlier biophysical study.[6] Importantly, most quadruplex ligands do not display such selectivity, but rather recognize a broad spectrum of quadruplex structures. Such ligands, while useful in some applications, could lead to undesired effects such as an increase in genome instability or in telomerase processivity if used as drugs.[47]

Parallel and antiparallel GQs formed by Tel22 in K^+ and Na^+ buffers, respectively, differ in loop positions and, possibly, positions of the metal ions within the GQ core. The terminal 3′ G-tetrad in parallel Tel22 GQ is unobstructed and provides an excellent place for ligand binding. In contrast, in the antiparallel basket form of Tel22, both terminal G-tetrads are hindered either by lateral loops that form an obstructing A·T Watson−Crick base pair or by the diagonal loop that runs across the terminal G-tetrad and whose bases stack onto it.[3] The blocked terminal G-tetrads of the antiparallel quadruplex call into question the binding mode of ligands with broad quadruplex specificity. It may be possible for a ligand to displace the obstructing bases of the loops or to bind to other features of the G-quadruplex. This latter explanation has been invoked for TOxaPy, an acyclic mimic of telomestatin.[48] In contrast to NMM, TOxaPy is selective for the antiparallel over the parallel Tel22 GQ. TOxaPy most likely binds to GQ grooves that are present in the antiparallel form of the human telomeric GQ but that are blocked by the external propeller loops in the parallel form. The comparison between TOxaPy and NMM indicates that selectivity for specific GQ topologies is possible and that proper GQ ligand design requires understanding of the molecular details of ligand−GQ interactions.

Potassium ions are known to be positioned between the G-tetrads as is observed here (Figure 3). Such positioning creates sufficient space to accommodate the *N*-Me group, and the distance between this group and K^+ is 3.7 Å. Na^+ ions have a smaller ionic radius as compared to K^+ ions and could be positioned within the G-tetrad, coplanar with the guanines. This is indeed observed in the crystal structures of the $d(TG_4T)$ quadruplex where the inner Na^+ ions are almost equidistant from the two G-tetrads, while the outermost Na^+ is positioned within a terminal 3′ G-tetrad.[49−52] This Na^+ ion is also coordinated to a water molecule in the axial position. If such positioning holds true in the antiparallel structure of Tel22 (even without considering the axial water molecule), the Na^+ ions would be sufficiently high up in the channel to cause steric clashes with the *N*-Me group, precluding NMM binding to this form of GQ and thus leading to the observed parallel versus antiparallel GQ selectivity.

The Role of the *N*-Me Group and NMM's Selectivity. In the crystal structure of Ni(II)- and Cu(II)-salphen compounds with a human telomeric GQ, the metal atoms are located almost directly above the ion channel.[17] Similarly, in the BRACO-19 structure, the positively charged ring nitrogen is in line with the potassium ions.[20] In both cases, the observed positioning can be justified by the cationic nature of the metal ion or nitrogen, which mimics the K^+ ions. The position of the *N*-Me group of NMM directly above the potassium channel of G-quadruplex is perplexing. The ion channel might merely provide a space for the *N*-Me group, allowing the porphyrin to stack onto the 3′ G-tetrad without steric clashes (note, other closest contacts of *N*-Me group are with the carbonyl oxygens, 3.3, 3.3, 3.4, and 3.5 Å). In contrast, such interaction is not possible with the duplex base pairs, thus leading to the GQ versus dsDNA selectivity observed in FRET melting studies[6] and in equilibrium dialysis experiments.[53]

The *N*-Me group plays another important role; it distorts the planarity of the NMM macrocycle, making this molecule more susceptible to further distortions induced by interacting biomolecules.[45] It is commonly accepted that nonplanarity of a porphyrin can be induced either by peripheral or core substitution or by interactions with proteins.[54] The amount and type (saddled, ruffled, domed, waved, and propeller) of porphyrin distortion can be quantified using the NSD method pioneered by Shelnutt.[40] The total out-of-plane deviation (D_{oop}) of the NMM macrocycle is 0.727 Å in **1** and 0.747 Å in **2** (Table 3 and Table S2). The NSD analysis indicates that

Table 3. NSD Results for Various NMM and MIX Models

ligand	D_{oop} (Å)	% domed[a]
NMM **1**	0.7273	34.6
NMM **2**	0.7469	43.7
$NMM_{solution}$	1.0677	22.7
NMM_{gas}	1.0442	23.3
NMM_{2Q3J}	1.8391	9.2
NMM_{1C1H}	1.5809	22.4
MIX_{frozen}	0.7279	34.6
$MIX_{solution}$	0.0461	11.0
MIX_{gas}	0.0501	12.4

[a]% domed is equivalent to d_{oop} domed divided by the sum of d_{oop} for all components multiplied by 100. 1C1H and 2Q3J are PDB IDs for WT and H138A mutant of ferrochelatase.

NMM is predominantly domed, with 34.6% and 43.7% domed character for **1** and **2**, respectively, Figure 6a. Other significant nonplanar deformations are wave(x) for **1** (28.3%) and **2** (22.5%) and saddled for **1** (20.0%). Doming deformation of the porphyrin can also be seen in the clothesline plot shown in Figure 6b; all of the pyrrole nitrogen atoms of NMM face downward, whereas the β-carbon atoms are distorted slightly upward. As expected, the pyrrole ring that hosts *N*-Me group is the most distorted.

Out-of-plane distortions are also observed in the G-tetrads, especially the one interacting with NMM, Figure 6b. The carbonyl groups of the 3′ G-tetrad (e.g., the O6 group) point down toward the center of the quadruplex, while the peripheral atoms, N2, C2, N3, C4, and N9, point up, forming an inverted dome-like shape with a total D_{oop} of 1.85 Å. The middle tetrad is significantly less distorted (D_{oop} = 1.08 Å), and the 5′ G-tetrad that forms the dimer interface is nearly planar (D_{oop} = 0.49 Å). The distortion of the 3′ G-tetrad allows for optimized $\pi-\pi$ stacking with nonplanar NMM, but it does not result from the interaction of this G-tetrad with NMM. A similar degree and type of distortion is seen in the 3′ G-tetrad of native Tel22 (Figure 6b, gray line, rmsd 0.241 Å) and Tel22 complexed with other ligands.

The observed domed geometry of NMM is either already present in its solution structure or is induced by its binding to

dx.doi.org/10.1021/ja3088746 | J. Am. Chem. Soc. 2012, 134, 20446−20456

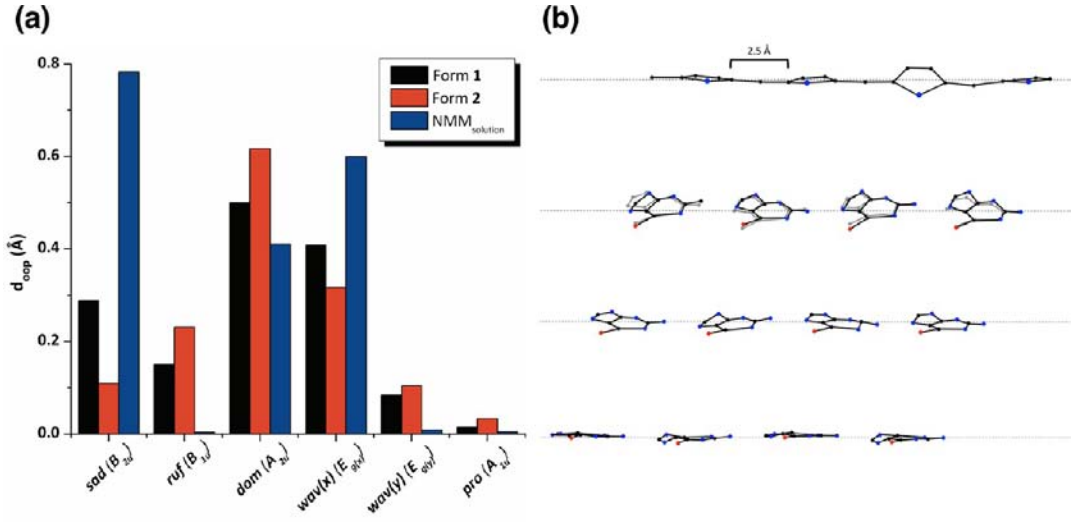

Figure 6. Nonplanar deformations of NMM in the Tel22−NMM complex. (a) NSD results for NMM in crystal forms **1** (black) and **2** (red), and for the optimized solution-phase structure (blue). NSD results for optimized gas-phase NMM are similar to the solution-phase structure and are not shown. (b) Principal component analysis results show the out-of-plane (oop) deviations for individual atoms of the NMM macrocycle and the three G-tetrads. The oop deviations for the 3′-terminal G-tetrad of the native Tel22 structure (1KF1) are shown in gray. The G-tetrads are offset horizontally and vertically (not to scale) to mimic the right-hand helical stacking of the GQ.

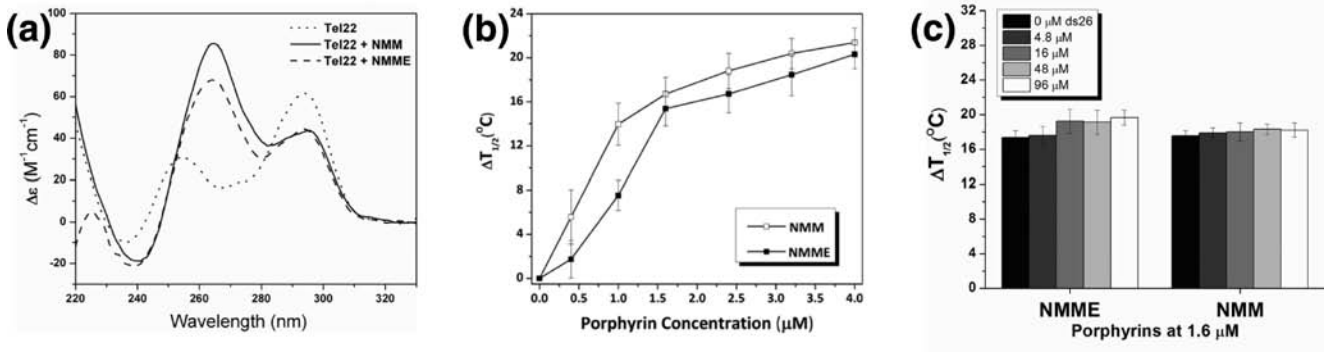

Figure 7. NMME interacts with Tel22 in a manner similar to that of NMM. (a) CD spectra of 3.0 μM Tel22 alone (dotted line) and in the presence of 6.0 μM NMM (solid line) or NMME (dashed line) in 5K buffer. Samples were annealed at 90 °C for 10 min, cooled slowly to 30 °C, and stored at this temperature for 12 h before collecting CD data at 25 °C. (b) Increase in the stabilization temperature, $\Delta T_{1/2}$, of the fluorescently labeled Tel22 analogue, F21D, in FRET melting assays as a function of porphyrin concentration. (c) Stabilization of 0.2 μM F21D by NMM or NMME in the presence of duplex DNA competitor, ds26.

the dome-shaped 3′ G-tetrad of Tel22. It is expected that NMM in solution is nonplanar due to the steric strain imposed by the *N*-Me group, although, to the best of our knowledge, there is no experimental structure of NMM alone. Therefore, we calculated energy-minimized structures of NMM in the gas and solution phases starting from the NMM's coordinates in the NMM−Tel22 crystal form **1** (Figure S7a). Alone, NMM displays significant saddled, domed, and wave(x) out-of-plane deviations (Figure S7d and Table S2). A similar geometry for NMM (albeit with overall higher deformation) was reported in a resonance Raman study.[55] When NMM structure is compared to that bound to Tel22, the former is significantly more nonplanar (D_{oop} = 1.068 vs 0.727) and saddled (43.2% vs 20.0%), and significantly less domed (22.7% vs 34.6%), Figure 6a. Thus, geometry of NMM changes upon its binding to Tel22, possibly, to optimize its $\pi-\pi$ stacking with the distorted 3′ G-tetrad. NSD analysis of NMM bound to wild-type[45] and H183A mutant[56] of *Bacillus subtilis* ferrochelatase indicates a predominantly saddled conformation of NMM (31.0% for wild-type and 40.1% for H138A mutant, Figure S7e) required to fit the binding pocket of this protein. Therefore, ferrochelatase, similar to Tel22, imposes a specific geometry on NMM.

The observed flexibility of NMM is facilitated by the presence of the *N*-Me group, which causes nonplanar deviation of the porphyrin macrocycle and decreased conjugation. Further distortion of NMM macrocycle, required for efficient binding to Tel22, comes at low energetic cost of only 0.7 kcal mol^{-1} (see Supporting Information). MIX (Figure 1c) has the same macrocycle structure as NMM, but lacks the *N*-Me group. This porphyrin was unable to stabilize Tel22 in FRET melting assays.[6] To understand why this is the case, energy minimization was performed on NMM structure with the *N*-Me group replaced by a hydrogen atom as a model for MIX (Figure S7b). The resulting structure is practically planar (D_{oop} = 0.046) and is approximately 4.3 kcal mol^{-1} more stable than "frozen" MIX, a structure that is forced to stay in the geometry adopted by NMM within the crystal structure (see the Supporting Information). Therefore, a large energy investment is required to distort the macrocycle of MIX to match the geometry of the 3′ G-tetrad of Tel22. In conclusion, the crystal

dx.doi.org/10.1021/ja3088746 | J. Am. Chem. Soc. 2012, 134, 20446−20456

structure of the NMM−Tel22 complex questions the commonly accepted requirement for a good GQ ligand to have a planar extended aromatic core, as the interaction of such ligands with Tel22 may be less efficient due to the ligand's inability to optimize its $\pi-\pi$ stacking with the distorted terminal G-tetrad.

The Role of the Propionate Groups. Under physiological conditions, the propionates of NMM are likely deprotonated and may repel the DNA backbone, opposing the stabilizing $\pi-\pi$ stacking and weakening the overall interaction between NMM and Tel22. This argument was used to explain NMM's relatively modest binding constant of $\sim 10^5$ M^{-1}.[6] Interestingly, the model of NMM used in this work to fit the observed electron density suggests that propionates may be involved in hydrogen bonding with the GQ backbone and that one of the carboxylates may be protonated, Figure S6a. To understand the role of propionates in NMM binding to Tel22, we performed CD annealing and FRET melting studies on the dimethyl ester of NMM (NMME). NMME is a neutral derivative of NMM and was chosen for these experiments because it cannot be deprotonated. Similar to NMM, NMME induced structural transition from a mixed hybrid to a parallel conformation of Tel22 in CD annealing studies (Figure 7a). In FRET melting assays, NMME exhibited stabilization of human telomeric DNA comparable to that of NMM and, just like NMM, displayed excellent selectivity toward GQ versus dsDNA (Figure 7b and c). The only advantage NMM has over NMME is its water solubility. These results taken together suggest that the possible negative charge of the propionate groups does not contribute significantly to, or detract significantly from, the binding or selectivity of NMM or its ability to induce structural conversion of Tel22.

To further test the effect of protonation state of the propionates on the strength of NMM interactions with Tel22, we determined the binding affinity at three different pH values: $(1.0 \pm 0.3) \times 10^5$ M^{-1} at pH 7.2,[6] $(1.2 \pm 0.1) \times 10^5$ M^{-1} at pH 5.8, and $(0.3 \pm 0.1) \times 10^5$ M^{-1} at pH 8.6; see Figure S8. The binding affinity remains virtually unchanged in the pH range 5.8−7.2 and drops only slightly at pH 8.6, suggesting that either the protonation state of the propionates does not change in this pH range or that the protonation state does not significantly affect the affinity of NMM for Tel22 in agreement with the conclusion reached above.

It is commonly accepted that increased ionic strength weakens an interaction between a ligand and a biological molecule if this interaction, at least in part, is electrostatic in nature. To test the effect of ionic strength on NMM−Tel22 interactions, we performed CD wavelength and melting experiments under ionic strength from 15 to 410 mM and a constant amount of KCl, 5 mM. The data indicate that the stabilization temperature, $\Delta T_{1/2}$, due to the presence of NMM is independent of the ionic strength up to 110 mM, and then it decreases only slightly (from 7 to 6 °C), Figure S9. Taken together, all biochemical data point to the predominantly nonelectrostatic nature of the NMM−Tel22 interactions.

■ CONCLUSIONS

The quadruplex binding ligand NMM displays unique selectivity not only for GQ versus dsDNA but also for a parallel versus antiparallel GQ. The X-ray crystal structure of human telomeric DNA bound to NMM reveals the molecular details underlying this selectivity. NMM is unusual in that its mode of binding does not involve electrostatic attractions of the sort observed for the majority of GQ-stabilizers. Rather, it relies on optimized $\pi-\pi$ stacking and complementarity between the *N*-Me group and a "hole" left by the K^+ ion channel in the center of the Tel22 GQ structure. It is not entirely clear if the latter interaction is merely an avoidance of steric clashes, or a true attraction, based, possibly, on the favorable electron density distribution between the ligand and Tel22 GQ. This specific recognition of the *N*-Me group by the interacting G-tetrad can explain the selectivity of NMM for GQ versus dsDNA and for parallel versus antiparallel GQ folds. Neither duplex DNA nor antiparallel GQ (possibly with a Na^+ ion within the terminal G-tetrad) have sufficient space to accommodate the *N*-Me group of NMM and thus cannot bind to this ligand.

Our previous biochemical characterization of NMM binding to Tel22 was insufficient to explain why MIX, a planar derivative of NMM, could not effectively stabilize Tel22.[6] The model of the NMM−Tel22 complex presented here suggests that the energetic barrier to the structural adjustment of MIX required for its optimal interaction with Tel22 is too high (4.3 kcal mol^{-1} for MIX versus 0.7 kcal mol^{-1} for NMM).

It has been shown previously that GQ DNA can undergo structural changes to optimize ligand binding, as in the case of the X-ray structure of BRACO-19 with a bimolecular GQ[20] and the NMR structure of *c-myc* GQ with a quindoline ligand.[57] Here, we report for the first time that a ligand, NMM, is also capable of adjusting its geometry (from saddled to domed) upon GQ binding. The complementarity of the surface of the terminal 3′ G-tetrad with NMM's macrocycle and its *N*-Me group leads to observed selectivity and to a 1:1 binding stoichiometry. Although it is widely believed that the extended aromaticity of the ligand is vital for its $\pi-\pi$ interactions with a G-tetrad, our data suggest that the ability of the ligand to adjust its geometry to closely match that of the interacting G-tetrad is equally important. Telomestatin, the gold standard of a selective GQ ligand, has an extended, but not rigid, aromatic system that may explain its efficient $\pi-\pi$ overlap with a quadruplex.

We have previously described that NMM induced structural isomerization of Tel22 in low K^+ conditions from a mixed-hybrid to a parallel structure.[6] Here we showed that Tel22 imposed domed geometry on NMM. Combined, these data indicate that both Tel22 and NMM have the ability to change geometry/topology in order to take part in their very special interactions. Both NMM and Tel22 undergo "adaptive binding", a term frequently used in the aptamer field. It will be of interest to determine how NMM interacts with the original mixed-hybrid structure of Tel22 to trigger its isomerization, and whether the NMM structural distortion occurs after the Tel22 isomerization is complete. Overall, NMM provides an important prototype for the development of truly selective GQ ligands, and our structural data will help inform further developments in this area.

On a final note, N-substituted porphyrins are interesting in their own right because of their unusual asymmetric distortion from planarity. Our data add to the basic structural understanding of the nonplanar geometry of NMM and show for the first time that this geometry can be modified further by the presence of interacting DNA molecule. Overall, the distortion of the porphyrin macrocycle has been proposed to be one of the most important factors that determines the chemical and electronic properties of porphyrins and, hence, their functions in living organisms.[58] Investigating and understanding these

small yet critical structural differences will help uncover biological roles of various porphyrin compounds.

■ ASSOCIATED CONTENT

Supporting Information

Description of additional experimental details and calculations, a table of all NSD parameters, figures for Beer's Law experiment on NMME, hydrogen-bonding network in crystal form **1**, concentration dependence of melting transition of Tel22, overlay of reported Tel22 structures, comparison of NMM and TMPyP4 binding to human telomeric GQ, details of interaction between propionates and Tel22 GQ, structure and nonplanar deviations in NMM, MIX, and transition state of NMM, a UV−vis titration of NMM with Tel22 at pH 8.6, CD experiments that test ionic strength effect on NMM−Tel22, and coordinates for all calculated porphyrin structures. This material is available free of charge via the Internet at http://pubs.acs.org.

■ AUTHOR INFORMATION

Corresponding Author

lyatsun1@swarthmore.edu

Present Address

[||]Department of Chemistry and Chemical Biology, Harvard University, 12 Oxford Street, Cambridge, Massachusetts 02138, United States.

Notes

The authors declare no competing financial interest.

■ ACKNOWLEDGMENTS

This work was supported in part by the Camille and Henry Dreyfus Faculty Start-up Award. We thank other members of the Yatsunyk group for discussions and help with manuscript revisions, Dr. Brad Johnson from the University of Pennsylvania for inspiring us to work with NMM, and Dr. Amy C. Rosenzweig from Northwestern University for help with X-ray data collection.

■ REFERENCES

(1) Phan, A. T. *FEBS J.* **2010**, *277*, 1107.
(2) Parkinson, G. N.; Lee, M. P. H.; Neidle, S. *Nature* **2002**, *417*, 876.
(3) Wang, Y.; Patel, D. J. *Structure* **1993**, *1*, 263.
(4) Heddi, B.; Phan, A. T. *J. Am. Chem. Soc.* **2011**, *133*, 9824.
(5) Renciuk, D.; Kejnovska, I.; Skolakova, P.; Bednarova, K.; Motlova, J.; Vorlickova, M. *Nucleic Acids Res.* **2009**, *37*, 6625.
(6) Nicoludis, J. M.; Barrett, S. P.; Mergny, J. L.; Yatsunyk, L. A. *Nucleic Acids Res.* **2012**, *40*, 5432.
(7) Monchaud, D.; Teulade-Fichou, M. P. *Org. Biomol. Chem.* **2008**, *6*, 627.
(8) Georgiades, S. N.; Abd Karim, N. H.; Suntharalingam, K.; Vilar, R. *Angew. Chem., Int. Ed.* **2010**, *49*, 4020.
(9) Shi, D.-F.; Wheelhouse, R. T.; Sun, D.; Hurley, L. H. *J. Med. Chem.* **2001**, *44*, 4509.
(10) De Cian, A.; Lacroix, L.; Douarre, C.; Temime-Smaali, N.; Trentesaux, C.; Riou, J.-F.; Mergny, J.-L. *Biochimie* **2008**, *90*, 131.
(11) Liu, Y.; Lin, C.; Li, H.; Yan, H. *Angew. Chem., Int. Ed.* **2005**, *44*, 4333.
(12) Qin, H.; Ren, J.; Wang, J.; Wang, E. *Chem. Commun.* **2010**, *46*, 7385.
(13) Alzeer, J.; Vummidi, B. R.; Roth, P. J. C.; Luedtke, N. W. *Angew. Chem., Int. Ed.* **2009**, *48*, 9362.
(14) Lubitz, I.; Zikich, D.; Kotlyar, A. *Biochemistry* **2010**, *49*, 3567.
(15) Parkinson, G. N.; Cuenca, F.; Neidle, S. *J. Mol. Biol.* **2008**, *381*, 1145.
(16) Collie, G. W.; Promontorio, R.; Hampel, S. M.; Micco, M.; Neidle, S.; Parkinson, G. N. *J. Am. Chem. Soc.* **2012**, *134*, 2723.
(17) Campbell, N. H.; Karim, N. H.; Parkinson, G. N.; Gunaratnam, M.; Petrucci, V.; Todd, A. K.; Vilar, R.; Neidle, S. *J. Med. Chem.* **2012**, *55*, 209.
(18) Collie, G. W.; Sparapani, S.; Parkinson, G. N.; Neidle, S. *J. Am. Chem. Soc.* **2011**, *133*, 2721.
(19) Bazzicalupi, C.; Ferraroni, M.; Bilia, A. R.; Scheggi, F.; Gratteri, P. *Nucleic Acids Res.* **2012**, DOI: 10.1093/nar/gks1001.
(20) Campbell, N. H.; Parkinson, G. N.; Reszka, A. P.; Neidle, S. *J. Am. Chem. Soc.* **2008**, *130*, 6722.
(21) Parkinson, G. N.; Ghosh, R.; Neidle, S. *Biochemistry* **2007**, *46*, 2390.
(22) Ren, J.; Chaires, J. B. *Biochemistry* **1999**, *38*, 16067.
(23) Cuenca, F.; Greciano, O.; Gunaratnam, M.; Haider, S.; Munnur, D.; Nanjunda, R.; Wilson, W. D.; Neidle, S. *Bioorg. Med. Chem. Lett.* **2008**, *18*, 1668.
(24) Moorhouse, A. D.; Santos, A. M.; Gunaratnam, M.; Moore, M.; Neidle, S.; Moses, J. E. *J. Am. Chem. Soc.* **2006**, *128*, 15972.
(25) Li, Y.; Geyer, R.; Sen, D. *Biochemistry* **1996**, *35*, 6911.
(26) Arthanari, H.; Basu, S.; Kawano, T. L.; Bolton, P. H. *Nucleic Acids Res.* **1998**, *26*, 3724.
(27) Paramasivan, S.; Bolton, P. H. *Nucleic Acids Res.* **2008**, *36*, e106.
(28) Hershman, S. G.; Chen, Q.; Lee, J. Y.; Kozak, M. L.; Yue, P.; Wang, L.-S.; Johnson, F. B. *Nucleic Acids Res.* **2008**, *36*, 144.
(29) Smith, J. S.; Johnson, F. B. *G-Quadruplex DNA* **2010**, 207.
(30) Cantor, C. R.; Warshaw, M. M.; Shapiro, H. *Biopolymers* **1970**, *9*, 1059.
(31) Leslie, A. *Acta Crystallogr., Sect. D: Biol. Crystallogr.* **2006**, *62*, 48.
(32) Adams, P. D.; Grosse-Kunstleve, R. W.; Hung, L.-W.; Ioerger, T. R.; McCoy, A. J.; Moriarty, N. W.; Read, R. J.; Sacchettini, J. C.; Sauter, N. K.; Terwilliger, T. C. *Acta Crystallogr., Sect. D: Biol. Crystallogr.* **2002**, *58*, 1948.
(33) Emsley, P.; Cowtan, K. *Acta Crystallogr., Sect. D* **2004**, *60*, 2126.
(34) Murshudov, G. N.; Vagin, A. A.; E. J., D. *Acta Crystallogr., Sect. D: Biol. Crystallogr.* **1997**, *53*, 240.
(35) DeLano, W. L. *PyMOL*; DeLano Scientific: San Carlos, CA, 2002.
(36) Becke, A. D. *J. Chem. Phys.* **1993**, *98*, 1372.
(37) Tomasi, J.; Mennucci, B.; Cammi, R. *Chem. Rev.* **2005**, *105*, 2999.
(38) Hratchian, H. P.; Schlegel, H. B. *J. Chem. Phys.* **2004**, *120*, 9918.
(39) Frisch, M. J.; et al. *Gaussian 09*, revision A.02; Gaussian, Inc.: Wallingford, CT, 2009.
(40) Jentzen, W.; Song, X.-Z.; Shelnutt, J. A. *J. Phys. Chem. B* **1997**, *101*, 1684.
(41) De Cian, A.; Guittat, L.; Kaiser, M.; Saccà, B.; Amrane, S.; Bourdoncle, A.; Alberti, P.; Teulade-Fichou, M.-P.; Lacroix, L.; Mergny, J.-L. *Methods* **2007**, *42*, 183.
(42) Terwilliger, T. C.; Grosse-Kunstleve, R. W.; Afonine, P. V.; Moriarty, N. W.; Zwart, P. H.; Hung, L. W.; Read, R. J.; Adams, P. D. *Acta. Crystallogr., Sect. D: Biol. Crystallogr.* **2008**, *64*, 61.
(43) Langer, G.; Cohen, S. X.; Lamzin, V. S.; Perrakis, A. *Nat. Protoc.* **2008**, *3*, 1171.
(44) Feng, Z.; Chen, L.; Maddula, H.; Akcan, O.; Oughtred, R.; Berman, H. M.; Westbrook, J. *Bioinformatics* **2004**, *20*, 2153.
(45) Lecerof, D.; Fodje, M.; Hansson, A.; Hansson, M.; Al-Karadaghi, S. *J. Mol. Biol.* **2000**, *297*, 221.
(46) Phan, A. T.; Kuryavyi, V.; Gaw, H. Y.; Patel, D. J. *Nat. Chem. Biol.* **2005**, *1*, 167.
(47) De Cian, A.; Cristofari, G.; Reichenbach, P.; De Lemos, E.; Monchaud, D.; Teulade-Fichou, M.-P.; Shin-ya, K.; Lacroix, L.; Lingner, J.; Mergny, J.-L. *Proc. Natl. Acad. Sci. U.S.A.* **2007**, *104*, 17347.
(48) Hamon, F.; Largy, E.; Guédin-Beaurepaire, A.; Rouchon-Dagois, M.; Sidibe, A.; Monchaud, D.; Mergny, J. L.; Riou, J. F.; Nguyen, C. H.; Teulade-Fichou, M. P. *Angew. Chem., Int. Ed.* **2011**, *50*, 8745.
(49) Phillips, K.; Dauter, Z.; Murchie, A. I. H.; Lilley, D. M. J.; Luisi, B. *J. Mol. Biol.* **1997**, *273*, 171.

(50) Laughlan, G.; Murchie, A.; Norman, D.; Moore, M.; Moody, P.; Lilley, D.; Luisi, B. *Science* **1994**, *265*, 520.
(51) Lee, M. P. H.; Parkinson, G. N.; Hazel, P.; Neidle, S. *J. Am. Chem. Soc.* **2007**, *129*, 10106.
(52) Creze, C.; Rinaldi, B.; Haser, R.; Bouvet, P.; Gouet, P. *Acta Crystallogr., Sect. D* **2007**, *63*, 682.
(53) Ragazzon, P.; Chaires, J. B. *Methods* **2007**, *43*, 313.
(54) Ma, J.-G.; Zhang, J.; Franco, R.; Jia, S.-L.; Moura, I.; Moura, J. J. G.; Kroneck, P. M. H.; Shelnutt, J. A. *Biochemistry* **1998**, *37*, 12431.
(55) Jarzecki, A. A.; Spiro, T. G. *J. Phys. Chem. A* **2004**, *109*, 421.
(56) Karlberg, T.; Hansson, M. D.; Yengo, R. K.; Johansson, R.; Thorvaldsen, H. O.; Ferreira, G. C.; Hansson, M.; Al-Karadaghi, S. *J. Mol. Biol.* **2008**, *378*, 1074.
(57) Dai, J.; Carver, M.; Hurley, L. H.; Yang, D. *J. Am. Chem. Soc.* **2011**, *133*, 17673.
(58) A. Shelnutt, J.; Song, X.-Z.; Ma, J.-G.; Jia, S.-L.; Jentzen, W.; Medforth, C. *Chem. Soc. Rev.* **1998**, *27*, 31.